

Numerical Simulations of Earthquake Cycles Using Depth-Dependent Frictional Parameters

Laarni S. dela Cruz
Institute of Mathematics
University of the Philippines
Diliman, Quezon City
dlaarni@math.upd.edu.ph

Kazuro Hirahara
Department of Geophysics
Kyoto University
Kyoto, Japan
hirahara@kugi.kyoto-u.ac.jp

ABSTRACT

Numerical simulations of earthquake cycles using a rate- and state-dependent friction law were performed on a segmented strike-slip fault such as the Philippine Fault Zone in Luzon. Frictional parameters were assigned to characterize stable and unstable zones along depth. The effect of normal stress history was also considered to provide some insights on the mechanics of earthquake cycles. The time evolution of shear stress, slip velocity, frictional coefficient, a state variable and displacement are calculated using a fifth-order Runge-Kutta method with an adaptive time step. Time histories of shear stress in the seismogenic zone over the entire duration of simulation were used to analyze fault interactions and seismically active periods obtained from the simulations.

1. INTRODUCTION

Earthquakes represent a great destructive force in an area especially in urban centers and preliminary simulations needed to develop hazard assessment systems is essential for risk reduction. Phenomena related to earthquakes occur over large scales of space and time. Simulations of earthquake cycles offer an analytical and predictive way of understanding data related to earthquakes rather than focusing on descriptive approaches that only involves observational data which only represent a portion of the system.

Rate- and state-dependent friction laws can simulate more realistic and complicated sliding behavior than simpler friction laws. It had been used to model seismic cycles at relatively simple plate boundaries such as the models presented

by [17], [31], [37] and [39]. Along strike-slip faults, a depth-dependent pore pressure distribution to generate complex earthquake cycles numerically, was presented by [4], [16] examined the effect of spatial variations of characteristic slip distance on complex slip pattern and earthquake statistics and, [19] performed a numerical simulation of seismic cycles or earthquake cycles along a bent, branched and segmented strike-slip model fault that is similar in geometry to the Xianshuihe fault but did not consider the perturbation of normal stress applied to the fault plane due to slip. [20] quantified the dependence of friction to normal stress history with a parameter α .

The complex tectonic setting of the Philippines justifies its vulnerability to earthquakes. The Philippine Fault Zone (PFZ) which traverses the entire archipelago has been seismically active and is associated with large earthquakes including the 1990 Luzon earthquake and this paper presents preliminary numerical models using a rate- and state-dependent friction law, on segmented strike-slip faults, with depth-dependent frictional parameters to characterize stable and unstable zones along depth, and considers the effect of normal stress history to provide some insights on the mechanics of earthquake cycles along the Philippine Fault Zone in Luzon. We also hope to emphasize the need for more studies to determine observational data sets required in numerical simulations of earthquake cycles such as recurrence intervals and active faults.

2. FAULT SEGMENTATION

Luzon is a plate boundary deformation zone situated across two opposing subduction zone and island arcs which accommodates the convergence of the Philippine Sea Plate and Sundaland Plate (see Figure 1). To invert block rotation rates that will characterize deformation in Luzon Island, Philippines, [14] used Global Positioning System and earthquake slip vectors as observed data. A fault and block system was utilized to describe zones of deformation. The system is composed of finite, elastic blocks, separated by discrete faults, basically a small-scale analog to the global model of plate tectonics. The initial micro-plate of Luzon is consist of seven blocks but the best model obtained from their computations only involves six blocks disregarding an assumed boundary of two blocks making Northern Cordillera Fault terminates at the Digdig Fault junction (see Figure 2). The motion of the PFZ is driven by the subduction of the Philippine Sea Plate and the Sundaland Plate from the east and the west respectively. Hence, it would be better to

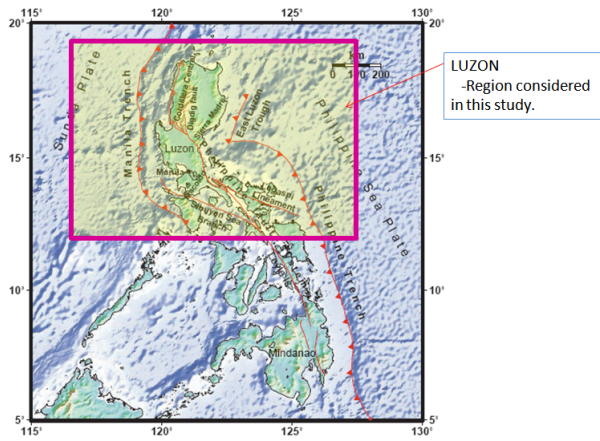


Figure 1: The Island of Luzon. Figure from [5].

consider such driving force directly to simulate earthquake cycles. The blocks suggested in [14] has boundaries which include the PFZ. Therefore, we use the block rotation rates estimated by [14] to determine the appropriate loading velocity on each fault segment.

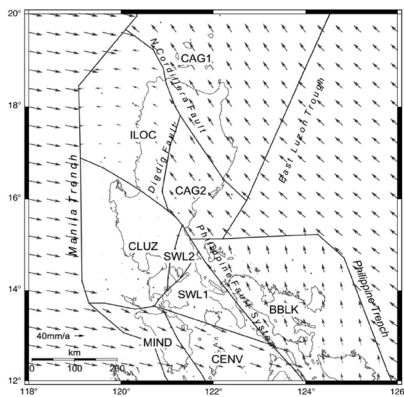


Figure 2: The preferred Luzon block model in [14]. This best-fit model consists of six mobile elastic blocks with varying rates of rotation. Arrows indicate direction of motion. Note that northeastern Luzon, depicted by blocks CAG1 and CAG2, behaves as 1 block, i.e., the Northern Cordillera Fault terminates at the Digdig Fault junction. Figure from [14].

Figure 3 shows a segmentation of the PFZ in Luzon. It is composed of nine segments and is based on the block boundaries in Figure 2 that corresponds to the PFZ in Luzon. The segmentation is an estimate of the mapped PFZ in Luzon shown in Figure 1. Horizontal lines along the fault indicate the division of the zone into segments. The surface trace of a segment is represented by a line. Green circles in Figure 3 indicate the location of historical earthquakes obtained from [3]. Table 1 presents the length of each segment used for the simulations.

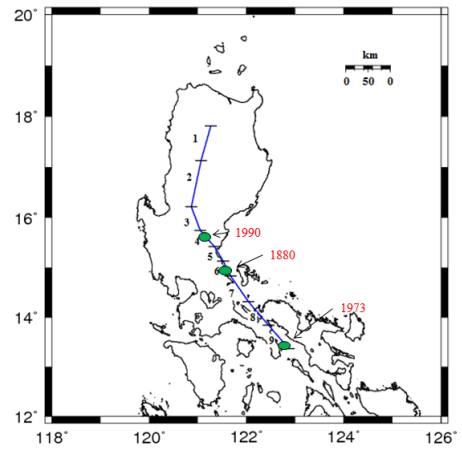


Figure 3: The model fault considered in the simulation of earthquake cycles in Luzon. The segmentation in this model is based on the block boundaries used in [14] along the PFZ. Horizontal lines along the fault indicate the division of the PFZ into segments. Green circles indicate the location of historical earthquakes obtained from [3].

Segment on the PFZ	Length of Segment (km)
Segment 1 (S1)	78.89
Segment 2 (S2)	104.31
Segment 3 (S3)	55.65
Segment 4 (S4)	47.40
Segment 5 (S5)	37.77
Segment 6 (S6)	37.64
Segment 7 (S7)	68.99
Segment 8 (S8)	69.28
Segment 9 (S9)	69.33

Table 1: Length of each segment.

3. MODEL

Each fault segment of the segmentation in Figure 3 is represented by a vertical fault plane with three discrete large cells along depths. Figure 4 shows that a fault segment or vertical fault plane is divided into three zones to represent the upper stable, seismogenic and lower stable zones of the Earth's crust. The seismogenic zone is also referred as the unstable zone. Each zone on a segment is represented by a cell with length equal to the length of the segment. Cells on the upper stable, seismogenic and lower stable zones have widths of 5 km, 20 km and 10 km respectively. The reference point for each cell is its center. This paper considered a discrete cell model in contrast to the continuous model of [31], because the PFZ in Luzon is quite long and this will require huge computations if the continuous model is used. [31] gives a bound for the cell size in order to satisfy continuum conditions along a vertical strike-slip fault. A rate- and state-dependent friction law was used to simulate earthquake cycles in a homogeneous elastic semi-infinite medium.

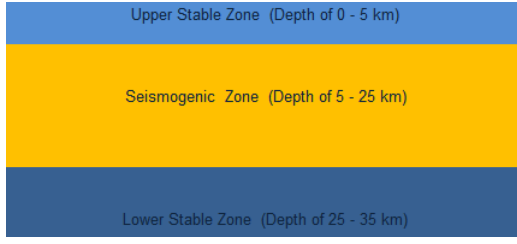


Figure 4: A fault segment or vertical fault plane is divided into three zones. Each zone on a segment is represented by a cell with length equal to the length of the segment. Cells on the upper stable, seismogenic and lower stable zones have widths of 5 km, 20 km and 10 km respectively. The reference point for each cell is its center.

The rate- and state-dependent constitutive formulation describes characteristic dependencies of friction on slip or displacement, slip velocity, slip history, and normal stress history observed in laboratory studies, and it provides a unified framework for predictive modeling of the various sliding phenomena observed for faults in nature and in the laboratory. The widely used formulation for resistance in sliding is developed in [33] and is written,

$$\tau = \sigma\mu, \text{ where} \quad (1)$$

$$\mu = \mu_0 + a \ln \frac{V}{V_0} + b \ln \frac{V_0\theta}{L}, \quad (2)$$

τ is the shear stress, σ is the normal stress and μ is the coefficient of friction; μ_0 , a and b are frictional parameters; V is slip velocity, θ is a state variable that evolves with slip and normal stress history, and L is a characteristic slip distance for renewal of contact population; V_0 is the reference velocity, μ_0 is the frictional coefficient at V_0 , t is time and α is a parameter that quantifies the effect of normal stress history on friction. The value of μ_0 for the Earth's crust ranges from 0.6–0.7. The state variable θ has the dimension of time and is interpreted to be a measure of the age of contact population between sliding surfaces, which evolve with contact time, slip, and normal stress history [8, 9, 10]. Friction in fault zones is dependent on slip velocity. Velocity weakening means that the friction gets smaller and velocity strengthening means that the friction gets bigger, as the slip velocity gets bigger, for some range of velocities. The parameter a characterizes the rise of friction as a response to sudden jump in slip velocity ([11],[32],[34]) and b characterizes the fall of friction after the jump in slip velocity. Hence $a - b < 0$ indicates velocity weakening behavior which promotes unstable sliding and $a - b > 0$ indicates velocity strengthening which results in stable sliding.

Different empirical evolution laws for the state variable θ have been proposed by [6, 12, 33]. The evolution law that is used in this study expresses the time [8], displacement [33] and normal stress-dependent [12] effects on friction and is written,

$$\frac{d\theta}{dt} = 1 - \frac{\theta}{L}V - \frac{\alpha\theta}{b\sigma} \frac{d\sigma}{dt} \quad (3)$$

where, α is a constant with $0 \leq \alpha \leq \mu_0$. The parameter α quantifies the effect of normal stress history in the state

variable. An experimentally determined range for the value of α is given in [12] which is 0.25-0.50.

The variables μ_i , τ_i , θ_i , V_i and σ_i denote the frictional coefficient, shear stress, state variable, slip velocity and normal stress at cell i . The parameters a_i , b_i and L_i are the parameters a , b and L at cell i . For each cell i , Equations (1), (2) and (3) should be satisfied. The relation between shear stress τ and slip velocity V on each cell i at time t is,

$$\tau_i = \sum_{j=1}^E K_{ij}(Vp_jt - u_j) - \frac{G}{2c}V_i = \mu_i\sigma_i$$

where G is the rigidity of the medium or shear modulus which is 30 GPa, c is the shear wave velocity of the Earth's crust which is 3000 m/sec, K_{ij} is the static shear stress change at the center of the i th cell due to a unit slip at the j th cell, u_j is the displacement at the j th cell, Vp_j is the loading or plate velocity at cell j , and E is the total number of cells from all segments of the PFZ in Luzon. The term $Vp_jt - u_j$ is the slip deficit at cell j . Hence, if K_i is the stress change at cell i due to the slip deficit of all cells in the system then it is given by

$$K_i = \sum_{j=1}^E K_{ij}(Vp_jt - u_j).$$

The term $G/2c$ acts as a radiation damping approximation which is given in [31] to evaluate shear stress reduction due to high-speed seismic rupture. A more detailed description of radiation damping can be found in [18].

To consider the effect of variable normal stress, the term

$$\sum_{j=1}^E N_{ij}(Vp_jt - u_j)$$

where N_{ij} is the static normal stress change at the center of the i th cell due to a unit slip at the j th cell was included. Differentiating both Equations (1) and (2) with respect to t , we have the following differential equations which should be satisfied in each cell i ,

$$\frac{d\tau_i}{dt} = \frac{d\mu_i}{dt}\sigma_i + \frac{d\sigma_i}{dt}\mu_i \quad (4)$$

$$\frac{d\theta_i}{dt} = 1 - \frac{\theta_i V_i}{L_i} - \frac{\alpha\theta_i}{b\sigma_i} \frac{d\sigma_i}{dt} \quad (5)$$

$$\frac{d\sigma_i}{dt} = \sum_{j=1}^E N_{ij}(Vp_j - V_j) \quad (6)$$

$$\frac{d\mu_i}{dt} = \frac{a_i}{V_i} \frac{dV_i}{dt} + \frac{b_i}{\theta_i} \frac{d\theta_i}{dt} \quad (7)$$

$$\frac{du_i}{dt} = V_i \quad (8)$$

$$\frac{dV_i}{dt} = \frac{K_i - \frac{\sigma_i b_i}{\theta_i} \left[1 - \frac{\theta_i V_i}{L_i} - \frac{\alpha\theta_i}{b\sigma_i} \frac{d\sigma_i}{dt} \right] - \frac{d\sigma_i}{dt} \mu_i}{\frac{G}{2c} + \frac{\sigma_i a_i}{V_i}} \quad (9)$$

K_{ij} and N_{ij} are computed using routines in [25] and [26]. Time histories of the variables τ , θ , σ , μ and V are solved using a fifth order Runge-Kutta method with an adaptive time step control [28] in each cell i .

Frictional parameters were assigned to each cell i in order to differentiate stable and unstable zones of the fault plane. Model parameters were chosen such that the simulated earthquake cycles mimicked the assumed recurrence interval of earthquakes in each segment. Parameters a_i and b_i were assigned to cells on the seismogenic zone such that $a_i - b_i < 0$. On the other hand, parameters such that $a_i - b_i > 0$ were assigned to cells on the upper and lower stable zones. A characteristic distance of $L_i = 1$ cm was assigned to all cells. Moreover, parameters were assigned on the unstable zone such that $K_{ij} < K_{critical}$ where $K_{critical} = (b_i - a_i)\sigma_{eff_i}/L_i$ for $i \neq j$, and σ_{eff_i} is the effective normal stress at cell i [23]. The depth-dependent effective normal stress is given by $\sigma_{eff_i} = (\rho - \rho_w)gz_i$ where ρ is the mean density of rock, ρ_w is the density of water, g is the gravitational constant and z_i is the depth of the center of cell i . The initial value for the normal stress σ_i is σ_{eff_i} . For this computation, ρ is $2.8 \times 10^3 \text{ kg/m}^3$, $\rho_w = 1000 \text{ kg/m}^3$ and $g = 9.8 \text{ m/s}^2$. For each cell i , the initial value of the frictional coefficient μ_i is μ_o . Hence, the initial value of shear stress τ_i is $\mu_o\sigma_{eff_i}$. The reference velocity or the initial velocity V_o on all cells is the average of all Vp_j in the model which is 2.5 cm/yr . The experimentally determined range for the value of α is given in [17] which is $0.25-0.50$. The coefficient of friction for the Earth's crust ranges from 0.6 to 0.7 . In this paper, the values $\mu_o = 0.6$ and $\alpha = 0.3$ were used.

3.1 Model with $a=0.001$

A fixed value of $a = 0.001$ was assigned to all cells. The values $b = 0.0003$ and $b = 0.0001$ were assigned on cells on the upper stable zone and lower stable zone respectively. Table 2 gives the assigned values of b on the seismogenic zone of each segment such that the simulated earthquake cycles mimicked the assumed recurrence interval of earthquakes in each segment. The appropriate loading velocity Vp on each fault segment were obtained from the block rotation rates estimated by [14].

Table 2 presents the estimated recurrence interval of earthquakes for each segment in the model. S3 together with S4, if taken as one region, is the location of the 1990 Luzon earthquake and had been the subject of many studies which includes paleoseismic studies such as [40] which had estimated a recurrence interval of 600 years in the region involving these segments. Previous paleoseismic studies such as [7] obtained a recurrence interval of 300-400 years and some have considered a recurrence interval of 345 years if the 1990 and 1645 earthquakes are assumed to have occurred from the same source. The non-existence of significant earthquakes in S1 and S2 lead us to assume a longer recurrence interval as we go north from S3. S1 and S2 are northern extension of S3 and S4. Hence a longer recurrence interval for S1 than S2 were assigned. Two historical earthquakes had been recorded for S5 to S9. Though the 1880 earthquake of magnitude 7.4 is located at S6, this study will consider S5, S6 and S7 as a unit, hence a recurrence interval of 360 years is assumed for these segments. For S8 and S9, this study assume a longer recurrence interval of 460 years.

3.2 Model with $a=0.015$

Segment on the PFZ	Loading Velocity (Vp) m/year	Recurrence interval	b on the seismogenic zone of the segment
S1	0.0172	800 yrs.	0.0014840
S2	0.0177	700 yrs.	0.0013230
S3	0.0245	600 yrs.	0.0017320
S4	0.0314	600 yrs.	0.0012890
S5	0.0288	360 yrs.	0.0014760
S6	0.0239	360 yrs.	0.0015280
S7	0.0280	360 yrs.	0.0013495
S8	0.0305	460 yrs.	0.0013810
S9	0.0314	460 yrs.	0.0013810

Table 2: Parameters for the Model with $a=0.001$.

The model described in subsection 3.1 is modified by considering higher values of a and b . A fixed value of $a = 0.015$ was assigned to all cells in the upper stable zone and seismogenic zone, while $a = 0.025$ was assigned in the lower stable zones. The values $b = 0.01$ and $b = 0.005$ were assigned on cells in the upper stable zone and in the lower stable zone respectively. These values were based on the values presented in [31] which were experimentally determined. Table 3 gives the assigned values of b on the seismogenic zone of each segment such that the simulated earthquake cycles mimicked the assumed recurrence interval of earthquakes in each segment.

Segment on the PFZ	b on the seismogenic zone of the segment
S1	0.01522
S2	0.0151
S3	0.01538
S4	0.015115
S5	0.01513
S6	0.01515
S7	0.015115
S8	0.0151627
S9	0.0151627

Table 3: Parameters for the Model with $a=0.015$.

4. RESULTS AND DISCUSSIONS

In section 4.1, results obtained from the model with $a=0.001$ are used to describe seismically active periods, the effect of normal stress history and shear stress interactions of segments with different strikes and lengths. In section 4.2, time histories of shear stress obtained from using $a=0.001$ and $a=0.015$ are compared. The occurrence of an earthquake is indicated by a sudden drop in shear stress which is the product of normal stress and friction, hence it is sufficient to determine seismically active periods and analyze fault interactions with the time histories of shear stress in each segment.

4.1 Results using Model with $a=0.001$

Time histories of shear stress using the model with $a = 0.001$, in 9 segments are plotted for cells on the seismogenic zone from $t=0$ to $t=7000$ and is shown in Figure 5.

A sudden drop in shear stress indicates the occurrence of an earthquake on the segment. For each segment, the length of a cycle estimates the assumed recurrence interval of earthquakes on the segment.

Figure 6 shows the time histories of shear stress change (MPa) from $t=6000$ to $t=7000$ years. Successive seismically active periods of approximately 100 years are separated by periods of relative inactivity of approximately 200 years in duration. This paper has not yet considered validating if these seismically active periods corresponds to historically recorded active periods. Figure 6 also shows that the maximum stress change in this model is 20 MPa.

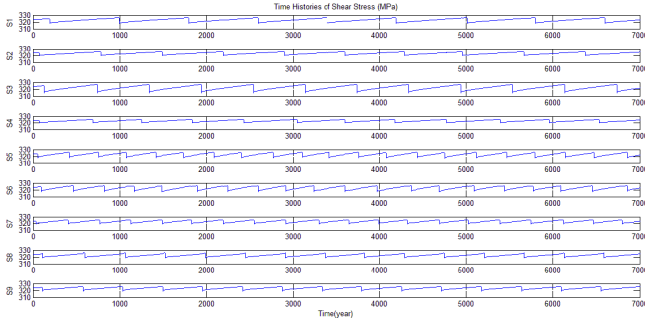


Figure 5: Time histories of shear stress using the model with $\alpha = 0.001$

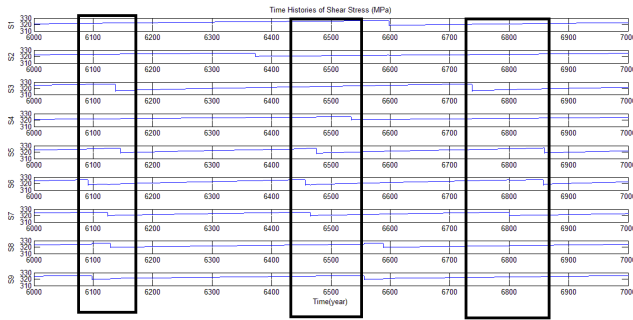


Figure 6: Time histories of shear stress change (MPa) from $t=6000$ years to $t=7000$ years. Successive seismically active periods (indicated by rectangular box) of approximately 100 years are separated by periods of relative inactivity of approximately 200 years in duration

The strike is an angle used to specify the orientation of a fault segment. The shear stress interactions between adjacent segments with the same strike, and adjacent segments with different strikes are shown in Figure 7(a) and 7(b) respectively. Figure 7(a) and Figure 7(b) are portions of the simulated earthquake cycles where ruptures or earthquakes have occurred on the considered segments. S8 and S9 have the same strike while S2 and S3 have different strikes. Figure 7(a) indicates that shear stress interaction is greater between 2 segments with the same strike. Shear stress drop in S9 causes an increase in shear stress in S8 while shear stress drop in S3 does not cause an increase in shear stress

in S2. This result validates the model since it is observed that adjacent fault segments of the same strike have more shear stress interaction than those with different strikes.

In Figure 8, S7 is larger than S6. A rupture in S6 resulted to an increase in shear stress in S7 but this is smaller compared to the increase in shear stress in S6 when a rupture occurred at S7. This shows that shear stress change in a segment with smaller length due to a rupture in a segment with larger length is bigger than the other way around.

Figure 7 and 8 show that the shear stress interaction is not so strong in this model. The weak shear stress interaction can be attributed to the calculated K_{ij} and N_{ij} . For cells i and j which are located on the same segment and have the same strike, the normal stress change N_{ij} is almost zero and $K_{ii} \gg K_{ij}$. For cells i and j located at different segments, $K_{ii} \gg N_{ij}$ and $K_{ii} \gg K_{ij}$. Hence, the seismic active period illustrated in Figure 6 are not mainly caused by segment interactions but more of a consequence of the assumed length of each cycle.

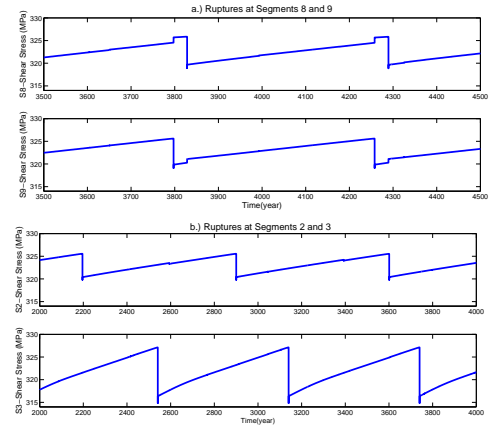


Figure 7: Shear stress interaction of two segments of a.) the same strike, shear stress drop in S9 causes an increase in shear stress in S8. and b.) different strikes, shear stress drop in S3 does not causes an increase in shear stress in S2.

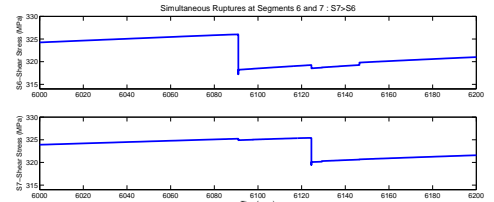


Figure 8: Time histories of shear stress between two segments with different lengths. Shear stress change in a segment with a smaller length due to rupture in a segment with a larger length is bigger than the other way around. In this figure, $S7 > S6$.

Figure 9 shows that the shear stress interaction of a curved fault does not have a significant difference when a parameter α is introduced. Hence, the effect of normal stress change in state evolution is then not so substantial in our simulations.

Additional information that can be obtained from the model include afterslips at the stable zones (see Figure 10). An earthquake in segment 4 is illustrated by the sudden increase of displacement in the seismogenic zone. Afterslip or displacement on the Earth's surface is manifested by the continuous displacement in the upper stable zone of segment 4 even after the occurrence of the earthquake.

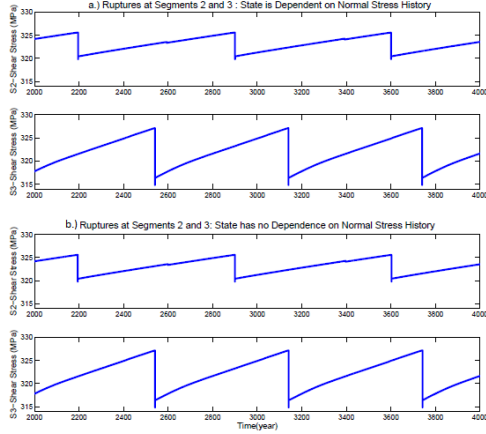


Figure 9: Effect of α on shear stress of two segments with different strikes where a.) $\alpha = 0.3$ (state is dependent on normal stress history) b.) $\alpha = 0$ (state has no dependence on normal stress history)

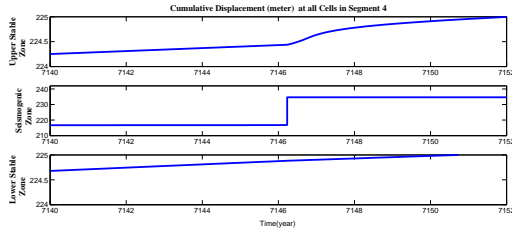


Figure 10: Afterslip in segment 4.

4.2 Results using Model with $a=0.015$

To illustrate the effect of a higher value of a to the earthquake cycle simulations, a value of $a = 0.015$ which is based on the value used in [31] was assigned. The results obtained for all the segments show that each segment took a longer time before the desired build-up of stress followed by the estimated recurrence interval of earthquakes are simulated (see Figure 11). For the time interval $t = 6000$ to $t = 7000$, observe the similarity in the number of ruptures in Figure 6 and Figure 11. Note that, the values of $a - b$ in the model with $a = 0.001$ and the model with $a = 0.015$ are almost equal. Hence, this result also shows that the value of $a - b$ may be more significant than the separate value of a and b .

5. CONCLUSIONS

Numerical simulations of earthquake cycles were performed using a rate- and state-dependent friction law, on a segmented strike-slip fault, with depth-dependent frictional parameters to characterize stable and unstable zones along depth, and considers the effect of normal stress history. It

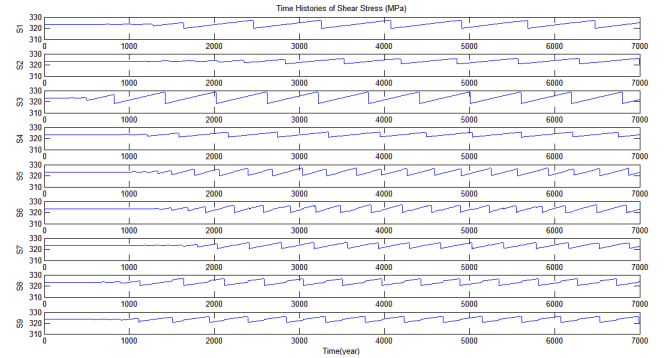


Figure 11: Time histories of shear stress using the model with $a = 0.015$.

was also able to provide some insights on the mechanics of earthquake cycles along the Philippine Fault Zone in Luzon. The PFZ in Luzon was divided into segments and the block rotation rates estimated in [14] were used to determine the appropriate loading velocity on each fault segment. The rate- and state-dependent friction law was used to simulate earthquake cycles in a homogeneous elastic semi-infinite medium. Frictional parameters were assigned to each cell to characterize different stable and unstable zones of the fault plane. Model parameters were chosen such that the simulated earthquake cycles mimicked the assumed or estimated recurrence interval of earthquakes.

It was shown that shear stress interaction is greater between adjacent segments with the same strike than adjacent segments with different strikes. It was also shown that the shear stress change in a segment with smaller length due to a rupture in a segment with larger length is bigger than the other way around. The shear stress interaction in the model output is not so strong. Hence, the seismic active periods that were determined are not mainly caused by segment interactions but more of a consequence of the assumed length of each cycle. The effect of normal stress change in state evolution is not so substantial since the shear stress interaction of a curved fault does not have a significant difference when a parameter α is introduced. It was also shown that the value of $a - b$ may be more significant than the separate value of a and b .

A different segmentation of the PFZ in Luzon is presented in [27] and is based on earthquake magnitudes. This different segmentation may result to a different duration of successive seismically active periods. Future computations may involve smaller cell size, a different segmentation, more established earthquake recurrence interval in each segment of the PFZ and the validation of computed seismically active periods with historically recorded active periods. Hence, this paper also emphasizes the need for more studies to determine observational data sets required in numerical simulations of earthquake cycles such as recurrence interval of earthquakes and active faults.

6. REFERENCES

- [1] H. ACHARYA, *Seismic Slip on the Philippine Fault and its Tectonic Implications*. *Geology* 8, 40–42, 1980.
- [2] E. AMIN, *Compilation of Damaging Earthquakes of the Philippines: Ragay Gulf Earthquake- 17 March 1973*, http://earthquake.phivolcs.dost.gov.ph/update_SOEPD/Earthquake/1973RagayGulfEQ/index-ragay.html (November 2008).
- [3] M.L. BAUTISTA, *Seismic Hazard Assessment of the Philippines Using Historical and Recent Earthquake Data*, Doctoral Dissertation, Kyoto University, 1998.
- [4] Y. BEN-ZION AND J.R. RICE, *Slip Patterns and Earthquake Populations along Different Classes of Faults in Elastic Solids*, *Journal of Geophysical Research* 100, 12 959–12 983, 1995.
- [5] J. BEAVAN, D. SILCOCK, M. HAMBURGER, E. RAMOS, C. THIBAUT, R. FEIR, *Geodetic Constraints on Postseismic Deformation following the 1990 Ms 7.8 Luzon Philippines Earthquake and Implications for Philippine Sea–Eurasian Plate Motion*. *Geochemistry, Geophysics, Geosystems* 2, 2001.
- [6] M.L. BLANPIED AND T.E. TULLIS, *The Stability and Behavior of a System with Two State Variable Constitutive Law*, *Pure and Applied Geophysics* 124: 415–444, 1986.
- [7] J. DALIGDIG, *Recent Faulting and Paleoseismicity along the Philippine Fault Zone, North Central Luzon, Philippines*, PhD thesis, faculty of Science, Kyoto University, 1997.
- [8] J.H. DIETERICH, *Modelling of Rock Friction. Part 1: Experimental Results and Constitutive Equations*, *Journal of Geophysical Research* 84(B5): 2161–2168, 1979.
- [9] J.H. DIETERICH, *Constitutive Properties of Faults with Simulated Gouge*. In: Carter NL, Friedman M, Logan JM, and Stearns DW (eds.) *Monograph 24: Mechanical Behavior of Crustal Rocks*, pp. 103–120. Washington, DC: American Geophysical Union, 1981.
- [10] J.H. DIETERICH AND B.D. KILGORE, *Direct Observation of Frictional Contacts: New Insights for Sliding Memory Effects*. *Pure and Applied Geophysics* 143: 283–302, 1994.
- [11] J.H. DIETERICH AND B.D. KILGORE, *Imaging Surface Contacts; Power Law Contact Distributions and Contact Stresses in Quartz, Calcite, Glass, and Acrylic Plastic*, *Tectonophysics* 256: 219–239, 1996.
- [12] J.H. DIETERICH AND M.F. LINKER, *Stability of Fault Slip Under Condition of Variable Normal Stress*, *Geophysical Research Letters* 19: 1691–1694, 1992
- [13] C.M.R. FOWLER, *The Solid Earth: An Introduction to Global Geophysics*, Cambridge University Press, 492pp.
- [14] G. GALGANA, M. HAMBURGER, R. MCCAFFREY, E. CORPUZ AND Q. CHEN. *Analysis of Crustal Deformation of Luzon Island, Philippines using Geodetic Observations and Earthquake Focal Mechanisms*, *Tectonophysics* 432:63-87. 2007.
- [15] J. GROTZINGER, T. H. JORDAN, F. PRESS, R. SIEVER, *Understanding Earth, Fifth Edition*, Freeman and Company. NY, 2005.
- [16] G. HILLERS, Y. BEN-ZION AND M. MAI, *Seismicity on a Fault with Rate- and State-Dependent Friction and Spatial Variations of the Critical Slip Distance*, *Journal of Geophysical Research*, 111, B01403, doi:10.1029/2005JB003859, 2006.
- [17] N. KATO AND T. HIRASAWA, *Nonuniform and Unsteady Sliding of a Plate Boundary in a Great Earthquake Cycle: A Numerical Simulation Using a Rate- and State-Dependent Friction Law*, *Pure appl. Geophys.*, 150, 425–442, 1999.
- [18] N. KATO AND T. TULLIS, *Radiation Damping as Approximation to Inertial Term for Dynamic Slip*, Brown University, http://www.geo.brown.edu/faculty/ttullis/Radiation_Damping.htm (July 2000).
- [19] N. KATO, L. XINGLIN AND W. XUEZE, *A Synthetic Seismicity Model for the Xianshuihe Fault, Southwestern China: Simulation Using a Rate- and State-Dependent Friction Law*, *Geophysical J. Int.* 169, 286–300, 2007.
- [20] M. F. LINKER AND J. H. DIETERICH, *Effects of Variable Normal Stress on Rock Friction: Observations and Constitutive Equations*, *Journal of Geophysical Research* 97, B4, 4923-4940, 1992.
- [21] C. MARONE, *Laboratory-derived Friction Laws and their Application to Seismic Faulting*, *Annu. Rev. Earth Planet. Sci.*, 26, 643–696, 1998.
- [22] A. MIKOLAJCIK, M. GLASSCOE, *The Southern California Integrated GPS Network Education Module*, Pasadena, US (CA) U.S. Geological Survey: Reston, US (VA) Jet Propulsion Laboratory (JPL), <http://scign.jpl.nasa.gov/learn/plate1.htm>.
- [23] N. MITSUI AND K. HIRAHARA, *Slow Slip Events Controlled by the Slab Dip and its Lateral Change along a Trench*, *Earth Planetary Science Letters*, 245, 344–385, 2006.
- [24] E. MORANTE, *The Ragay Gulf Earthquake of March 17, 1973, Southern Luzon, Philippines*, *Journal of Geological Society of the Philippines*, 28(2), 1974.
- [25] Y. OKADA, *Surface Deformation to Shear and Tensile Faults in a Half Space*. *Bulletin of the Seismological Society of America* 75: 1135–1154, 1985.
- [26] Y. OKADA, *Internal Deformation Due to Shear and Tensile Faults in a Half-space*, *Bulletin of the Seismological Society of America* 82 ,Issue: 2, Pages: 1018-1040, 1992.
- [27] PHIVOLCS, *The Metro Manila Earthquake Impact Reduction Study*, 2004.
- [28] W. H. PRESS, B. P. FLANNERY, S. A. TEUKOLSKY, AND W. T. VETTERLING, *Numerical Recipes, 2nd Ed.*, Cambridge Univ. Press, New York, 1992.
- [29] K. RANJITH AND J. R. RICE, *Stability of Quasi-static Slip in a Single Degree of Freedom Elastic System with Rate- and State-Dependent Friction*, *Journal of the Mechanics and Physics of Solids*, 47, 1999, pp. 1207-1218.
- [30] G. RANTUCCI, *Geological Disasters in the Philippines : The July 1990 Earthquake and the June 1991 Eruption of Mount Pinatubo*, Rome, IT, Oct. 1994 .
- [31] J. RICE, *Spatio-Temporal Complexity of Slip on a Fault*, *Journal of Geophysical Research (ISSN 0148-0227)*, vol. 98, no. B6, p. 9885-9907.

- [32] J. RICE, Class Lecture, *Introduction: Frictional Constitutive Laws, Physical Basis, Nucleation of Instability, and Dynamic Sliding in Earthquakes*, Harvard University, EPS 263, November 2006.
- [33] J. RICE AND AL. RUINA, *Stability of Steady Frictional Slipping*, Journal of Applied Mechanics 50: 343–349,1983.
- [34] G. SCHUBERT (ED), *Treatise on Geophysics* , 7000 pages, 11 volumes.
- [35] K. SHIMAZAKI AND T. NAKATA, *Time-Predictable Recurrence Model for Large Earthquakes*, Geophysical Research Letters, 7, 279–282, 1980.
- [36] S. STEIN, M. E. WYSESSION, *An Introduction to Seismology, Earthquakes, and Earth*, Wiley-Blackwell, 2003.
- [37] W. D. STUART, T. E. TULLIS, *Fault Model for Preseismic Deformation at Parkfield, California*, Journal of Geophysical Research 100, 24 079–24 099, 1995.
- [38] C. THIBAUT, *GPS Measurement of Crustal Deformation in the Northern Philippine Island Arc*, Master's Thesis, Department of Geological Sciences, Indiana University, Bloomington, Indiana. 923–926, 1999.
- [39] S.T TSE, J.R. RICE, *Crustal Earthquake Instability in Relation to the Depth Variation of Frictional Slip Properties*, Journal of Geophysical Research 91, 9452–9472, 1986.
- [40] H. TSUTSUMI ET. AL, *Timing of Surface-Rupturing Earthquakes on the Philippine Fault Zone in Central Luzon Island, Philippines*, American Geophysical Union, Fall Meeting 2006, abstract #T33A-0510, 12/2006.